Volume 2 | Number 5 | October 2015 | Pages 409–552

Environmental Science Nano

rsc.li/es-nano

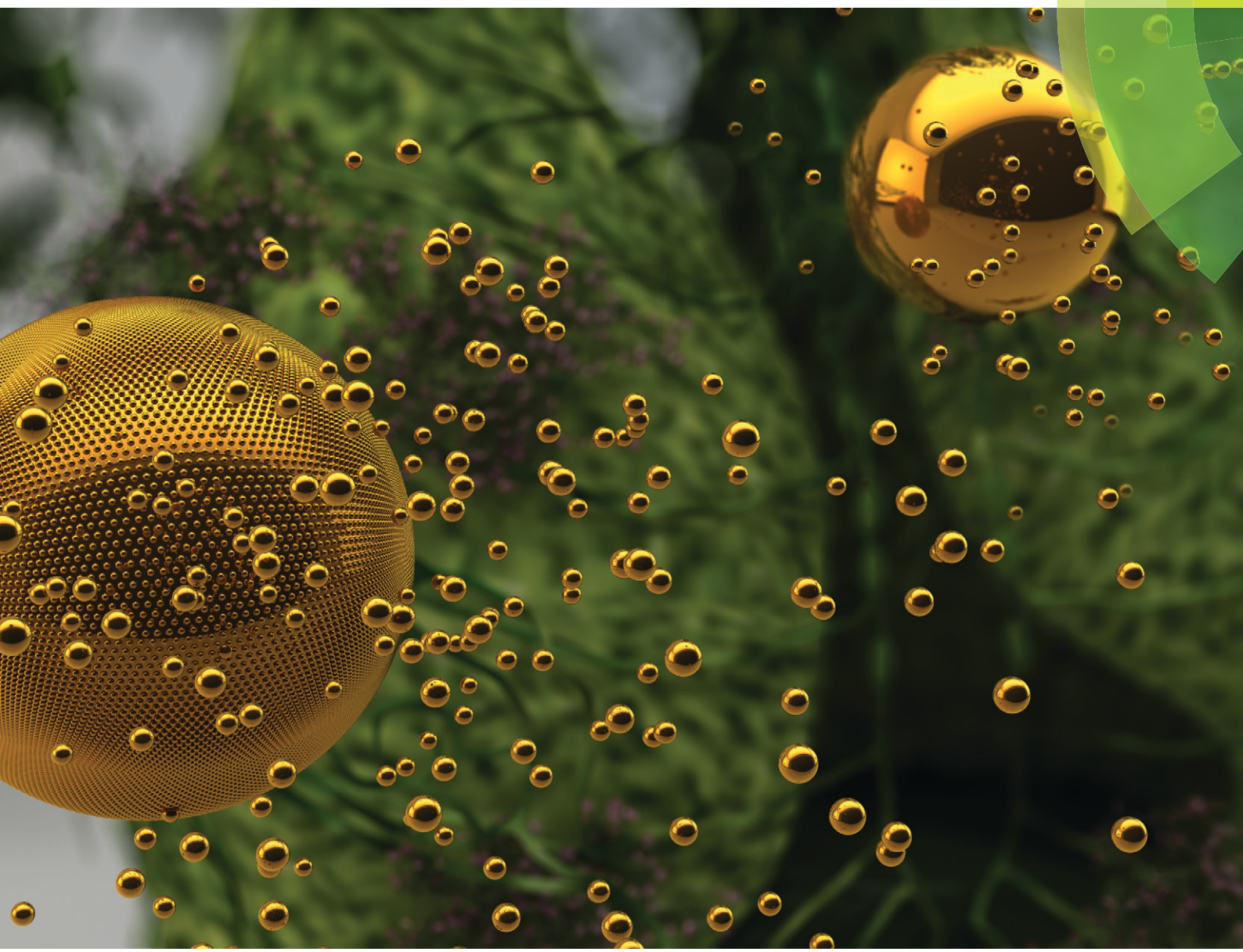

ISSN 2051-8153

ROYAL SOCIETY OF CHEMISTRY

PAPER

Peter J. Vikesland *et al.*

Room temperature seed mediated growth of gold nanoparticles: mechanistic investigations and life cycle assessment

Environmental Science Nano

PAPER

View Article Online
View Journal | View Issue

Cite this: *Environ. Sci.: Nano*, 2015, **2**, 440

Room temperature seed mediated growth of gold nanoparticles: mechanistic investigations and life cycle assesment†

Weinan Leng, Paramjeet Pati and Peter J. Vikesland*

Received 21st February 2015,
Accepted 2nd August 2015

DOI: 10.1039/c5en00026b

rsc.li/es-nano

In this study, we report the first room temperature seed-mediated synthesis of gold nanoparticles (AuNPs) in the presence of citrate and a gold salt. In contrast to citrate-reduction in boiling water, these mild reaction conditions provide expanded capacity to probe the mechanism of seed-mediated growth following gold salt addition. Moreover, comparative life cycle assessment indicates significant reductions in the environmental impacts for the room temperature synthesis. For this study, highly uniform gold seeds with *Z*-average diameter of 17.7 ± 0.8 nm and a polydispersity index of 0.03 ± 0.01 were prepared by a pH controlled protocol. We investigated the AuNP growth mechanism *via* time resolved UV-vis spectroscopy, dynamic light scattering, and transmission electron microscopy. This study indicates that citrate and its oxidation byproduct acetone dicarboxylate serve to bridge and gather Au(III) ions around gold nanoparticle seeds in the initial growth step.

Nano impact

Nanoparticle synthesis mechanisms are difficult to study given the fast rate of the physicochemical processes involved in the nucleation and growth of nanoparticles. A deeper mechanistic understanding will allow us to develop design rules for synthesizing nanoparticles with tightly controlled sizes and morphologies. Moreover, we need to incorporate principles of green chemistry and engineering into those design rules to improve conventional energy-intensive nanomaterial production practices. This paper describes the seed mediated synthesis of citrate-reduced gold nanoparticles at room temperature. This method allows us to probe the mechanisms involved therein, as well as reduces the life cycle environmental impacts of the production step. The mechanistic insights gained from this study can inform new green synthesis approaches for producing other nanomaterials.

Introduction

Nanotechnology holds immense promise for its capacity to address many societal problems. A key challenge in exploiting the novel properties of nanomaterials is in the synthesis of nanoparticles with precisely controlled sizes and morphologies. In addition, nanomaterial synthesis may involve multi-step, multi-solvent, energy intensive manufacturing processes[1,2] that may be associated with significant environmental impacts. Recently there have been increased efforts 1) to develop design principles to synthesize highly monodisperse nanoparticles[3,4] and 2) to incorporate the principles of green chemistry into nanomaterial synthesis.[5–7] In this paper, we present a novel approach for the room temperature seeded growth of gold nanoparticles (AuNPs) and compare its life cycle impacts with those of previously reported methods[8,9] that require high-temperature boiling.

AuNPs and their conjugates are particularly versatile nanomaterials.[10–12] Exhibiting low toxicity in biological systems,[13–15] AuNPs conjugated with drugs and peptides have been used to modulate pharmacokinetics and drug delivery, thus allowing for specific targeting of cancer cells and organelles.[16–21] The physical properties of AuNPs (*e.g.*, color, localized surface plasmon resonance (LSPR), electrical conductivity, *etc.*) are significantly enhanced when they are functionalized with appropriate metal or organic groups.[22] For example, aggregation induced changes in plasmon response can be coupled with colorimetric detection mechanisms to establish rapid analyte detection.[13,23–27] Such methods are promising in that they entail very simple sample handling procedures, minimum instrumental investment, and can be carried out in the field using portable devices.

The nanoscale properties of AuNPs are size- and shape-dependent,[11,28] and thus there has been an extensive effort to control AuNP size, shape, and surface composition while simultaneously maintaining narrow size distributions.[11,29–32]

Department of Civil and Environmental Engineering, Virginia Polytechnic Institute and State University, 418 Durham Hall, Blacksburg, VA 24060-0246, USA.
E-mail: pvikes@vt.edu

† Electronic supplementary information (ESI) available. See DOI: 10.1039/c5en00026b

The synthesis of gold nanoparticles by trisodium citrate (Na_3Ctr) mediated reduction of aqueous chloroauric acid ($HAuCl_4$),[8,9] is one of the most widely used AuNP synthesis strategies. This synthesis approach, involving rapid addition of Na_3Ctr into a hot aqueous solution of $HAuCl_4$, has been modified and optimized over many decades.[31,33–35] In this synthesis Na_3Ctr simultaneously acts as (i) reducing agent (driving the reduction of Au^{III} to Au^0),[9,33,36,37] (ii) capping agent (electrostatically stabilizing the AuNP colloidal solution),[37–39] and (iii) pH mediator (modifying the reactivity of Au species involved in the reaction).[31]

Room temperature syntheses of noble metal nanoparticles involving synthetic surfactant[40] and bio-based reductants and capping agents[41] have been previously reported. Seed-mediated growth of AuNPs has been shown to be especially effective in producing highly monodisperse AuNPs.[42,43] In this work, however, we discuss what we believe to be the first effort to examine seed-mediated AuNP growth in the presence of citrate and gold salt at room temperature. Highly uniform and reproducible gold seeds were prepared for seed-mediated growth using a pH-controlled protocol. By inoculating the growth medium with a controlled number of gold seeds, the particles produced *via* this approach have sizes varying from 20–110 nm with the final size dependent on the number of seeds and the total concentration of gold ions in the growth solution. Given the room temperature conditions, this seeded growth synthesis approach adheres to Principle 6 of the Green Chemistry Principles[44] (Design for Energy Efficiency), which recommends using ambient temperature and pressure whenever possible. The longer reaction times also offer new opportunities to probe the reaction mechanism and study the evolution of AuNP size and morphology.

Sustainability has been identified as an emerging design criterion in nanomaterial synthesis.[3] Incorporating green chemistry and engineering principles into nanoscience has been suggested as a proactive approach to mitigate the environmental impacts of nanotechnology.[5,6] However, green synthesis approaches for nanoparticle production may have unintended environmental impacts.[45] Life cycle assessment (LCA) is being increasingly used to study the environmental impacts of different nanotechnologies to assess tradeoffs and identify environmental hotspots therein.[46–50] For example, are reductions in the energy footprint of the AuNP synthesis process due to the milder room temperature conditions substantially larger than any increase in the energy use due to longer reaction times? To investigate this issue, we conducted an LCA study to compare the environmental impacts of the AuNP synthesis at room temperature as well as under boiling conditions.

Materials and methods

Materials

Gold(III) chloride trihydrate ($HAuCl_4{\cdot}3H_2O$) and trisodium citrate dihydrate ($Na_3Ctr{\cdot}2H_2O$) were purchased from Sigma-Aldrich (St. Louis, MO) at the highest purity grade available. Deionized water (18 MΩ cm) was used for all preparations. All glassware was cleaned in a bath of freshly prepared *aqua regia* (HCl/HNO_3, 3 : 1 v/v) and then rinsed thoroughly with deionized water prior to use. All reagent solutions were filtered through a 0.2 μm polycarbonate membrane prior to their use in AuNP synthesis.

AuNP seed preparation

Gold nanoparticles of ≈14 nm diameter were synthesized according to Frens *et al.*[8] with a slight modification for size and monodispersity control.[31] This synthesis involves chemical reduction of $AuCl_4^-$ at pH 6.2–6.5 by dissolved Na_3Ctr at 100 °C. In brief, 100 mL of 1 mM $HAuCl_4$ containing 200 μL of 1 M NaOH was prepared in a 250 mL flask equipped with a condenser. The solution was brought to boil while being stirred with a PTFE-coated magnetic stir-bar and 10 mL of 38.8 mM Na_3Ctr was rapidly added. The reaction was allowed to proceed until the solution attained a wine red color. After 15 min of reaction, the reflux system was shut down and deionized water was added to the AuNP seed suspension to bring the final volume to ≈100 mL. 'Room temperature synthesis' as used herein refers explicitly to the seed-mediated growth of AuNPs and not the synthesis of AuNP seeds. We utilized elevated temperatures for seed production as we found it to be the best way to control the monodispersity of the seeds. We note, however, that citrate-stabilized AuNP seeds may be synthesized by other methods that may or may not involve elevated temperatures.

Seed-mediated AuNP growth at room temperature

Growth reactions (40 mL final volume) were performed in a 100 mL Erlenmeyer flask. Briefly, a variable volume aliquot of seed suspension ($N = 6.54 \times 10^{12}$ particles per mL) and 227 μL of 44.7 mM $HAuCl_4{\cdot}3H_2O$ were added to the flask with water. Subsequently, a 176 μL aliquot of 38.8 mM $Na_3Ctr{\cdot}2H_2O$ was added to the flask under constant stirring. In these syntheses the only variable was the initial AuNP seed concentration (ESI† Table S1).

AuNP characterization

UV-vis spectra were acquired using a Cary 5000 UV-vis-NIR spectrophotometer. AuNP suspensions were placed in 1 cm sample cells and spectra between 400–800 nm were acquired at room temperature. For the time-dependent measurements of the seeded growth experiments, aliquots were removed and samples were probed within 2 min of reductant addition. At the same time, an aliquot of suspension was frozen at −20 °C. At this temperature the suspended nanoparticles precipitated out of the suspension. The thawed solution was centrifuged at 10 000 × *g* for 10 min, and the supernatant was used for UV-vis and ICP-MS analysis.

Gold nanoparticles were visualized using a Zeiss 10CA transmission electron microscope equipped with an AMT Advantage GR/HR-B CCD Camera System. Sample aliquots of 3 μL were drop-cast onto carbon-coated 100-mesh copper

grids (Electron Microscopy Sciences). After 5 minutes, the drop was wicked away using filter paper. The sample was then rinsed three times by inverting the TEM grid onto a drop of water for 5 seconds and then allowing the grid to dry face up. TEM images of the as prepared AuNPs were used for size distribution measurements. For each sample, the dimensions of >60 particles were quantified using NIH ImageJ software (version 1.44). Electrophoretic mobility and intensity based particle size distributions and hydrodynamic diameter were determined with a Zetasizer NanoZS instrument (Malvern Instruments, UK) with a 173° scattering angle at a temperature of 25 °C. A refractive index of 1.35 and an absorption value of 0.01 were used for the AuNPs.[51] Raman experiments were performed using a WITec alpha500R (Ulm, Germany). A 10× Olympus objective (NA = 0.3) was used to focus a 633 nm laser into a 2 mm flow cell. The Raman signal was collected using a 30 s integration time.

Size and concentration calculation of AuNPs

(1) Size and concentration of Au seeds. The average size of the gold seeds was calculated *via* TEM analysis. A TEM image of seeds synthesized *via* the pH controlled method is shown in Fig. 1. Using ImageJ, the average nanoparticle diameter (d_{seed}) was determined to be 13.9 ± 0.5 nm. Assuming a spherical particle and a reaction yield of 100%,[45] the number density of gold seeds (N_{seed} = 6.75 × 10^{12} particles per mL) was calculated based upon the known initial concentration of gold c_{Au} (mol L^{-1}):[52]

$$N_{seed} = \frac{6\times10^{21} C_{Au} M}{\pi \rho_{Au} d_{seed}^{3}} \quad (1)$$

where ρ is the density of gold (19.3 g cm^{-3}) and M is its atomic weight (197 g mol^{-1}). A similar concentration of 6.54 × 10^{12} particles per mL was calculated based upon the absorbance of the particle suspension at 450 nm (A_{450}) using the method reported by Haiss *et al.*[53]

$$N_{seed} = \frac{A_{450}\times10^{14}}{d_{seed}^{2}\left[-0.295+1.36\exp\left(-\left(\frac{d_{seed}-96.8}{78.2}\right)^{2}\right)\right]} \quad (2)$$

Given the similarity of these values and due to the possibility of overestimating the gold nanoparticle concentration

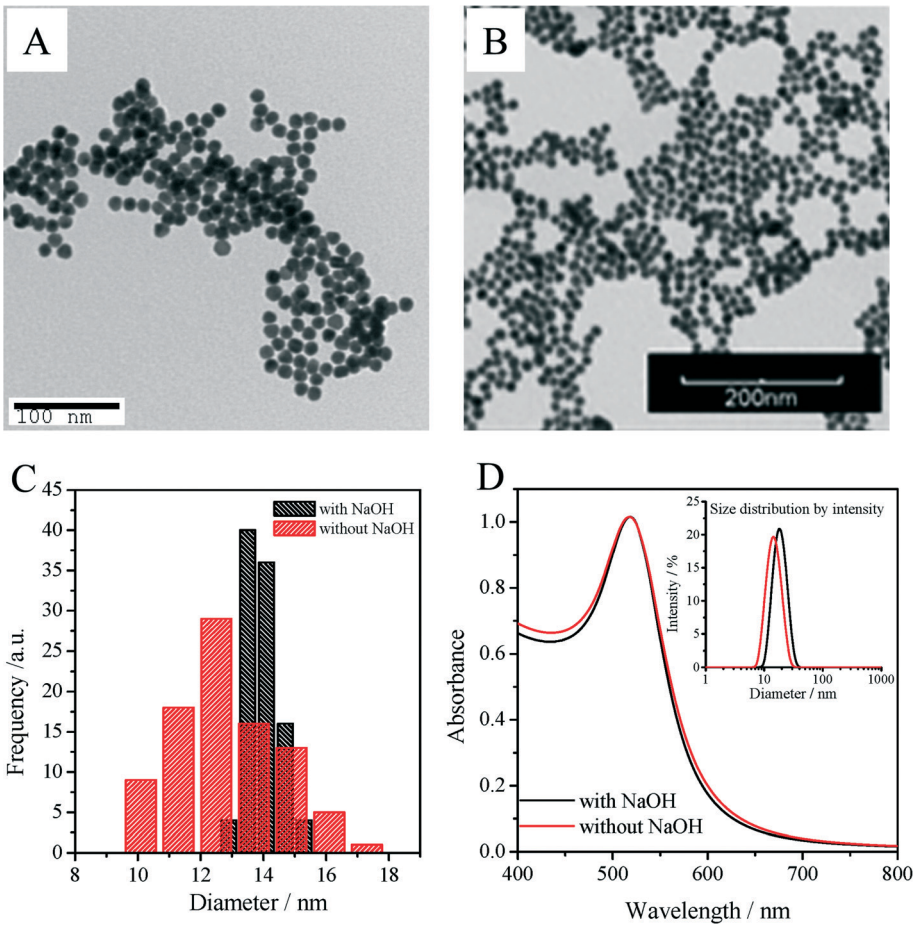

Fig. 1 TEM micrographs of seed nanoparticles synthesized by (A) pH controlled method and (B) w/o pH control; (C) TEM size distributions from both methods; (D) normalized absorption spectra and hydrodynamic size distribution by intensity (inset) of two seed suspensions with (black lines) and w/o pH controlled (red lines) procedures. Suspensions were diluted 3× and 9× for UV-vis and DLS measurements, respectively.

following filtration, a N_{seed} value of 6.54×10^{12} particles per mL as determined using the Haiss equation was used in all calculations.

(2) Size and concentration of seed mediated AuNPs. Assuming that (a) all of the gold precursor is consumed during the reaction, (b) the resultant AuNPs are spherical in shape, and (c) gold reduction and nanoparticle growth take place without nucleation of new 'seed' particles, the effective size of the grown particles can be quantitatively predicted.[54]

$$d_{AuNP}{}^3 = d_{seed}{}^3 + \frac{6\times10^{21} m_{Au}}{\pi \rho_{Au} n_{seed}} \quad (3)$$

where m_{Au} and n_{seed} are the Au mass (g) and the number of seed particles present during seed mediated growth. The number density of AuNPs (N_{AuNP}) is simply n_{seed} divided by the total volume (V) of the AuNP solution,

$$N_{AuNP} = \frac{n_{seed}}{V} \quad (4)$$

The molar concentration of the AuNP solutions was then calculated by dividing the number density of particles by Avogadro's constant (6.022×10^{23}).

Life cycle assessment (LCA) of AuNP synthesis methods

LCA is a quantitative framework used to evaluate the cumulative environmental impacts associated with all stages of a material – from raw material extraction through the end-of-life.[55] We conducted a cradle-to-gate comparative LCA of seeded-AuNP growth at room temperature and under boiling conditions. Our LCA models consider processes from raw material extraction ("cradle") and processing through the synthesis of the nanoparticles ("gate"). The functional unit is 1 mg of AuNP synthesized by each approach. The LCA models exclude purification steps and synthesis waste products. Furthermore, we did not consider recycle streams since it is not common practice to capture AuNP waste streams in laboratory scale synthesis.

The material and energy inventories for the AuNP synthesis were built using measured data from our laboratory. The average medium-voltage electricity mix for the US Northeast Power Coordinating Council was used to model energy use. The uncertainty for energy use was modeled as a uniform distribution with the maximum and minimum values being ±20% of the calculated energy use as per measurements performed in our laboratory. LCA models were constructed using SimaPro (version 8.0.4). The inventory for chemical precursors used in these syntheses was modeled using the EcoInvent database[56] (version 3.01).

Gold(III) chloride and sodium citrate were not found in the LCA inventory databases. Therefore, the synthesis of these two chemicals were modeled as custom-built processes using appropriate assumptions for yield and uncertainties as discussed elsewhere (Table S2†).[57] Life cycle impact assessment (LCIA) was done using the Cumulative Energy Demand (CED) method[56,58] (version 1.09) and the ReCiPe MidPoint method (version 1.11), using midpoints and the hierarchist (H) perspective with European normalization. CED estimates the embodied and direct energy use for materials and processes in the syntheses and gives a detailed energy footprint. The ReCiPe impact assessment method estimates life cycle impacts across a broad range of impact categories (*e.g.*, climate change, freshwater eutrophication, marine ecotoxicity, *etc.*). All uncertainty analyses were performed using Monte-Carlo simulations for 1000 runs. The uncertainty analyses include the uncertainties in the custom-defined processes in SimaPro, energy use in lab equipment and the unit processes in EcoInvent used in our LCA models. Fig. S1 and S2† show the chemicals and processes considered in the LCA models. The life cycle inventories are shown in Tables S2, S3, and S4.†

Results and discussion

Monodisperse AuNP seed production

Highly uniform and reproducible AuNP seeds were prepared *via* citrate reduction both with and without pH adjustment. In the traditional Turkevich/Frens' approach, nanoparticle size, nanoparticle polydispersity, and the overall reaction mechanism are determined by the solution pH set by $[Na_3Ctr]$.[31] Unfortunately, as the $Na_3Ctr/HAuCl_4$ ratio increases from 0 to 30 there is an increase in solution pH from 2.8 to 6.8 (Fig. S3, ESI†). Over this pH range, $AuCl_4^-$ undergoes pH-dependent hydrolysis to produce $[AuCl_x(OH)_{4-x}]^-$ (x = 0–4) complexes.[59] Due to the electron withdrawing capacity of the hydroxyl ligand increased gold ion hydroxylation results in an increase in standard reduction potential (Fig. S4, ESI†).[31,60,61] Past studies have shown that the final AuNP size can be tuned by changing the solution pH due to this effect.[31,60]

Addition of Na_3Ctr without pH control causes the solution pH to increase above 6.2 during the latter stages of AuNP synthesis. This change converts highly reactive $AuCl_3(OH)^-$ into less reactive complexes of $AuCl_X(OH)_{4-X}$ (X = 0–2), and the reaction pathway consists of a single nucleation-growth step.[31,61] Tight control of nanoparticle size is challenging under these conditions because growth and nucleation occur simultaneously during the early stages of Na_3Ctr addition (*i.e.*, when the pH $<$ 6.2). To address this issue during seed preparation we set the solution pH to a value of ≈6.4 by addition of 200 μL of 1 M NaOH to the reaction solution.

Fig. 1A shows a typical TEM micrograph for seed nanoparticles synthesized using our pH controlled synthetic protocol. The nanoparticles are highly monodisperse with a pseudo-spherical diameter of 13.9 ± 0.5 nm and an average aspect ratio (AR) of 1.06 ± 0.04. We also calculated average particle diameters using Haiss' eqn (11) (with B_1 = 3.00 and B_2 = 2.20),[53] based on the UV-vis spectra of the AuNP seeds. This particle diameter (13.6 ± 0.7 nm) closely matched the average particle size obtained from TEM measurements (13.9 ± 0.5 nm). The size distribution of 3.6% coincides with a highly reproducible DLS Z-average diameter and polydispersity index (PDI), 17.7 ± 0.8 nm and 0.03 ± 0.01, respectively,

for twelve replicate batches. Particles synthesized without pH control (*i.e.*, without adding NaOH) were also characterized (as illustrated in Fig. 1). For this synthesis, the pH value of 5.6 at the beginning of reaction was set by the $Na_3Ctr/HAuCl_4$ ratio alone (Fig. S3, ESI†). Compared with the pH controlled synthesis, an immediate color change (<1 min) of the reaction suspension was observed following Na_3Ct injection, while the pH controlled reaction required 2–3 min to see a similar color change, thus indicating faster nucleation and growth due to the higher reactivity of the gold complexes at elevated pH (Fig. S4, ESI†). Although Fig. 1D shows the two syntheses have very similar LSPR λ_{max} (517.9 nm for non pH controlled particles, 518.5 nm for pH controlled particles), the hydrodynamic diameter and TEM diameter of the nanoparticle increased from 15.2 nm to 17.7 nm and from 12.9 nm to 13.9 nm respectively as the pH increased from 5.6 to 6.4. Consistent with the broader TEM size distribution (Fig. 1C) and absorption peak width at half maximum[62] of

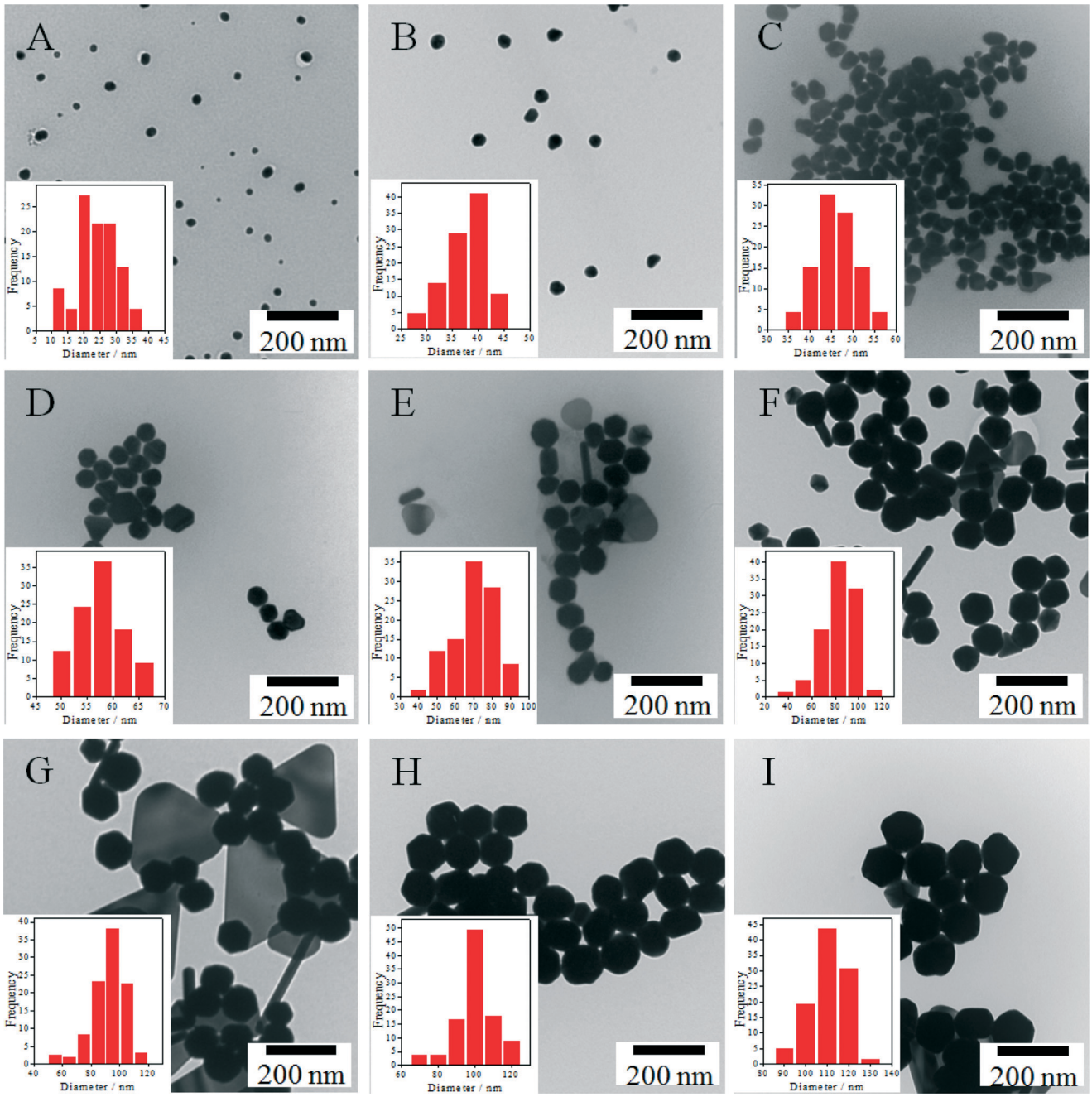

Fig. 2 TEM images of room temperature seed-mediated AuNPs of different sizes (aspect ratio): A) 24.0 ± 6.1 nm (AR: 1.15 ± 0.17), B) 37.1 ± 4.6 nm (AR: 1.15 ± 0.11), C) 46.0 ± 4.6 nm (AR: 1.34 ± 0.14), D) 57.6 ± 4.5 nm (AR: 1.14 ± 0.06), E) 69.6 ± 11.8 nm (AR: 1.13 ± 0.07), F) 82.5 ± 14.0 nm (AR: 1.13 ± 0.07), G) 92.4 ± 11.4 nm (AR: 1.15 ± 0.11), H) 100 ± 11.4 nm (AR: 1.11 ± 0.11), I) 111.0 ± 8.3 nm (AR: 1.11 ± 0.09). Inset: histograms of diameters as determined by NIH ImageJ software.

the LSPR band (Fig. 1D), a larger PDI of 0.19 was obtained for the non-pH controlled particles along with a 17% error between the particle size determined based upon the TEM measurements (12.9 nm) and the size calculated using the Haiss equation (10.7 nm). As the initial Au^{III} concentration and the $Na_3Ct/HAuCl_4$ ratio were both fixed for the two seed synthesis approaches, this finding is consistent with the previous observation that AuNP size and monodispersity of gold nanocrystals are strongly dependent on the initial pH of the reaction medium.[31]

Room temperature seeded growth of AuNPs

Because of the rapid reaction kinetics at 100 °C it is necessary to keep Au^{III} and the reductant apart during seed-mediated growth[63] and the order and speed of reagent addition strongly affect the final size and polydispersity of the nanoparticles.[62] To achieve improved nanoparticle homogeneity, we hypothesized that seeded growth could be carried out at room temperature – and could simply be initiated following addition of seed nanoparticles to premixed solutions of Au^{III} and reductant (or alternatively the introduction of Au^{III} to a mixture of reductant and seeds). As illustrated herein, such an outcome can be accomplished when the rate constant for surface mediated growth is significantly greater than the rate constant for nucleation – a condition that occurs at room temperature. As shown in Fig. 2, by inoculating the growth medium with a controlled number of gold seeds, the particles produced *via* this approach have sizes varying from 20–110 nm with the final size dependent on the number of seeds and the total concentration of gold ions in the growth solution. A majority of the NPs produced by this approach are quasi-spherical in shape, although nanocrystal triangles and rods also form in low yield (<13%) in the larger nanoparticle (>70 nm) preparations (Table S5†). Ignoring the presence of the non-spherical particles, the average diameters and concentrations of the particles were determined and are tabulated in Table 1. For this calculation, we assumed that all of the particles exhibit spherical geometries. However, as illustrated in Fig. 2 this assumption becomes increasingly incorrect for the larger nanomaterial sizes. We note that the similarity in particle size determined experimentally and predicted using eqn (3) suggests that nucleation of small nanoparticles does not occur, thus indicating that the final concentration of AuNPs correlates well with the initial number of AuNP seeds.

As indicated in Table 1 and Fig. S6A,† we determined the hydrodynamic diameter and size distribution of the AuNPs using DLS. The extreme sensitivity of the scattered signal to changes in the radius (R) of the scattering objects (scattered intensity $\propto R^6$),[64] enables DLS to detect the presence of even small numbers of aggregates in NP dispersions. The seeded AuNPs in our work are not true spheres and should be described as ovoid with one dimension elongated relative to the other. The effects of rotational diffusion result in the appearance of a false peak in a size range of about 5–10 nm during DLS measurement for size distribution by intensity.[65] This artifact causes the hydrodynamic size determined by DLS to be smaller than the TEM determined core size, a result consistent with production of AuNPs by seed-mediated growth at 100 °C.[66,67]

Gold nanoparticles display colors and LSPR bands in the visible spectral region that are dependent upon NP size and shape.[11,68,69] The origin of the LSPR band is the coherent excitation of free conduction electrons due to polarization induced by the electric field of the incident light. A change in the absorbance or wavelength of the LSPR band provides a measure of particle size, shape, as well as aggregation state. UV-vis measurements were obtained to provide additional characterization of the nanoparticle properties. In Fig. S6B,† we provide both optical images and normalized UV-vis spectra for AuNPs of different sizes. For nanoparticle diameters between 14 and 120 nm, the color exhibits a smooth transition from dark red to pink and ultimately to yellowish brown. As expected,[70] the LSPR wavelength is dependent on the nanoparticle size, as evinced by the increase of the maximum absorbance wavelength (λ_{max}) from 518 to 582 nm for nanoparticles of increasing size. This red shift is accompanied by

Table 1 Sizes, concentrations, zeta-potentials, and optical properties of seeded AuNPs

AuNP	SPR peak (nm)	Concentration (NPs per mL)[a]	Mean ξ potential (mV)	Diameter of AuNP (nm)		
				Calculated[b]	TEM[c]	*Z*-average/PDI (DLS)
A	525.9	5.5×10^{11}	−40.5 ± 1.2	22.7	24.0 ± 6.1	25.9/0.193
B	533.9	1.3×10^{11}	−40.2 ± 0.7	34.2	37.1 ± 4.6	25.0/0.53
C	536.5	5.4×10^{10}	−38.7 ± 1.1	45.7	46.0 ± 4.6	31.2/0.502
D	537.2	2.7×10^{10}	−40.7 ± 1.6	57.1	57.6 ± 4.5	45.9/0.314
E	541.2	1.6×10^{10}	−42.7 ± 0.5	68.6	69.6 ± 11.8	61.2/0.239
F	551.9	9.7×10^{9}	−43.5 ± 0.6	80.0	82.5 ± 14.0	79.2/0.162
G	561.2	6.5×10^{9}	−44.4 ± 1.5	91.4	92.4 ± 11.4	89.7/0.148
H	569.9	4.6×10^{9}	−42.2 ± 2.7	102.9	100.0 ± 11.4	97.8/0.113
I	581.9	3.3×10^{9}	−46.6 ± 1.4	114.3	111.0 ± 8.3	105.8/0.114

[a] Theoretical concentration of seeded AuNPs based upon the seed concentration and assuming that all gold salt precursors are reduced to gold atoms that condense onto the seed particle surface. [b] Particle sizes as determined using eqn (3) for a seed concentration of 6.54×10^{12} particles per mL. [c] For the particles with one dimension elongated, the sizes are overestimated by $[(AR)^{1/6} - 1] \times 100\%$. (where AR is the aspect ratio of the elongated particle).

the broadening of the LSPR band in the long wavelength region. This broadening may be due to an increase in polydispersity,[71] particle agglomeration,[31] or a combination of both processes. Samples left at room temperature in the dark often agglomerated and precipitated, but could be easily re-suspended by shaking or sonication. Such storage exhibited no effect on nanoparticle stability.

Monitoring seed-mediated AuNP growth process

During AuNP synthesis, Ctr^{3-} is oxidized to acetone dicarboxylate ($ACDC^{2-}$; eqn (5)), a ligand that complexes Au^{III}, thus facilitating nanoparticle growth. Following nanoparticle nucleation, $ACDC^{2-}$ is thought to be rapidly degraded to acetate at the synthesis temperature of ≈100 °C.[9]

$$2AuCl_4^- + 3Ctr^{3-} \rightarrow 2Au + 3ACDC^{2-} + 3CO_2\uparrow + 8Cl^- + 3H^+ \quad (5)$$

$$ACDC^{2-} + 2H_2O \xrightarrow{100\ °C} \text{acetone} + 2CO_2\uparrow + 2OH^- \quad (6)$$

Past studies suggest that $ACDC^{2-}$ or its degradation products take part in additional redox reactions when the $Na_3Ctr/HAuCl_4$ ratio is less than 1.5.[62] Of particular relevance is a model developed based upon the kinetics of the AuNP formation which suggests that acetone or other carboxylate byproducts formed by the degradation of $ACDC^{2-}$ (eqn (6)) reduce auric chloride and lead to its complete conversion to Au^0 (eqn (7)).[9,39]

$$4AuCI_4^- + 6H_2O + 3\ \text{acetone} \xrightarrow{100\ °C} 4Au + 9CH_2O + 12H^+ + 16CI^- \quad (7)$$

Summing up eqn (5)–(7) and correcting for the reaction stoichiometry provides the following:

$$2AuCl_4^- + Ctr^{3-} + 2H_2O \xrightarrow{100\ °C} 2Au + 3CH_2O + 3CO_2\uparrow + 8Cl^- + 3H^+ \quad (8)$$

This model, however, does not consider the effects of temperature on $ACDC^{2-}$ degradation. At room temperature it is known that $ACDC^{2-}$ undergoes slow oxidation in the presence of oxygen:[72]

$$2ACDC^{2-} + H_2O + 5.5O_2 \xrightarrow{\text{Room temp.}} 2CH_2O + HCOOH + 7CO_2 + 4OH^- \quad (9)$$

We speculate the following similar reaction occurs preferentially in the presence of Au^{III}:

$$6ACDC^{2-} + 22AuCl_4^- + 24H_2O \xrightarrow{\text{Room temp.}} 22Au + 6CH_2O + 3HCOOH + 21CO_2 + 88Cl^- + 54H^+ \quad (10)$$

By summing up eqn (5) and (10), the reaction stoichiometry in eqn (11) indicates that 1 mol of citrate can reduce >4 mol of $HAuCl_4$.

$$6Ctr^{3-} + 26AuCl_4^- + 24H_2O \xrightarrow{\text{Room temp.}} 26Au + 6CH_2O + 3HCOOH + 27CO_2 + 104Cl^- + 60H^+ \quad (11)$$

We note that both Ctr^{3-} and $ACDC^{2-}$ are carboxylates and that any byproducts of their oxidation, reduction, or degradation are likely to contain carboxylate groups.[73] Therefore, the carboxylate moiety is a likely means of interaction with the AuNP surface regardless of the exact species involved in AuNP capping.[74,75]

As noted previously, room temperature reaction conditions slow the AuNP synthesis reaction, thus allowing for improved opportunities to characterize the seeded growth process. At room temperature, the suspension color changed very slowly, but followed a similar sequence as the traditional process at elevated temperature (*i.e.*, from pale pink (seeds), to dark blue, to purple). Fig. 3 shows typical TEM images for different growth times for seed mediated AuNPs prepared at a $Na_3Ctr/HAuCl_4$ ratio of 0.67 and a seed concentration of 5.35×10^{10} particles per mL (this corresponds to the 'Type C' AuNPs in Table 1). As shown in Fig. S7,† the UV absorption of Na_3Ctr decreases dramatically following Au^{III} addition, thus indicating its rapid coordination with Au^{III}. In this synthesis, Na_3Ctr facilitates coordination of Au^{III} ions around the AuNP seeds. This coordination involves fast ligand exchange between the carboxylates and chlorine ions within the $AuCl_X(OH)_{4-X}$ complexes.[37]

Previous studies suggest that the mode of interaction between Na_3Ct and the AuNPs/Au ions is likely through a bidentate bridging mode or *via* unidentate or chelate modes.[39,76–78] As shown in Fig. 3A, within 2 minutes of mixing the AuNP seeds with Na_3Ctr and $HAuCl_4$ we observed formation of large (>100 nm) weakly associated clusters that consist of large numbers of AuNP seeds. These images are very similar to the large fluffy clusters observed by Chow and Zukoski in the early stage of AuNP synthesis at 60 °C.[35] Some of these crystallites may have formed following the drying of the suspension on the TEM grid. Nonetheless, this result suggests that carboxylates bound to the seed surface and present in the growth medium enhance the association between AuNP seeds and Au^{III} ions (Scheme 1). After 30 minutes the clusters are no longer observed and have broken apart due to the continued reaction between the carboxylates and Au^{III} and the suspension exhibits a light blue color. Fig. 3B shows irregular gold nanowires together with aggregates at this growth stage, a result similar to the observations by Ji *et al.*[31] and Pei *et al.*[79] for nanoparticles produced using Frens' method.[8] After 1 hour, the gold nanowires form fluffy spherical networks (diameter ≈ 100 nm; Fig. 3C). In Fig. 3C (inset), some irregular gold nanowires remain isolated from the larger network. As the reaction proceeds, however, the network continues to grow in size (Fig. 3D). Similar trends in

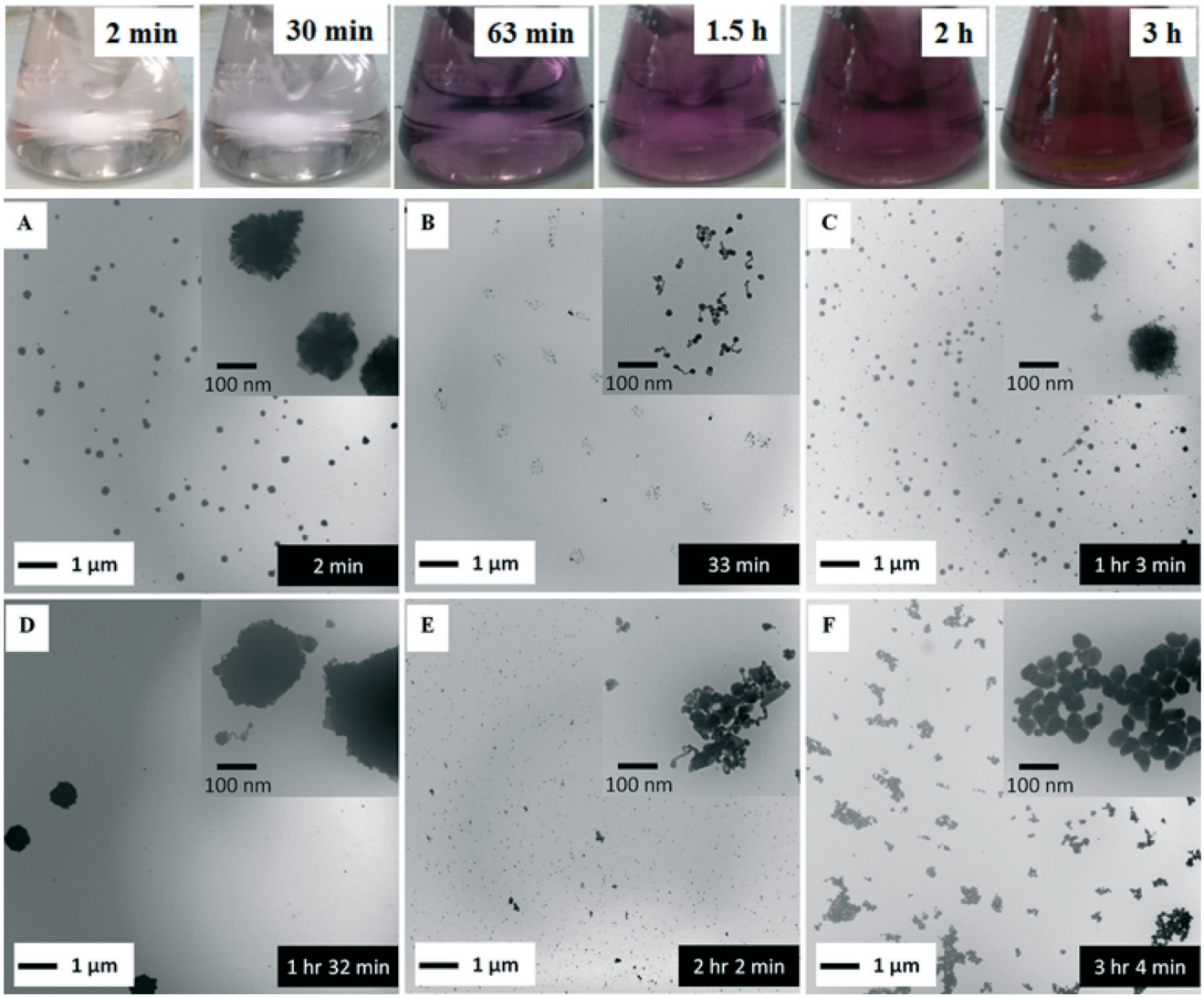

Fig. 3 Seed mediated growth of Type C (Table 1) AuNPs for a mixed solution of $HAuCl_4$ (0.254 mM), Au seeds (5.35×10^{10} particle per ml), and Na_3Ctr (0.17 mM) at room temperature. Panels A–F are TEM images of particles obtained at the different growth times indicated in the flask images across the top of the figure.

the AuNP synthesis progress at elevated temperatures have been reported by previous researchers.[35] After two hours, the fluffy network breaks apart into smaller segments (Fig. 3E). Ultimately, as the color of the reaction suspension changes color to purple-red, spherical nanoparticles with diameter of 30–40 nm cleave off of the nanowires (Fig. 3F). At the conclusion of the reaction, evinced by the unchanging particle diameter (Fig. 4B) and LSPR peak (Fig. 4C), the suspension attains a purple-red color and well-defined particles of 46 nm diameter are observed (Fig. 2C).

Aliquots of the reaction suspensions were extracted and monitored by DLS and UV-vis to further characterize the particle growth process depicted in Fig. 3. Fig. 4A illustrates the intensity weighted hydrodynamic size distributions determined by DLS at different growth stages. In addition to the peak for the seeded particles in the region of 10–100 nm, a small size distribution peak was detected after 1 hour of growth. This peak can be explained as a result of the formation of non-spherical particles with one dimension elongated relative to the other. The effects of rotational diffusion result in the appearance of a false peak in a size range of about 5–10 nm during DLS measurement.[65] The presence of this peak is also consistent with the TEM results in Fig. 3C–F that show that there is a small proportion of particles with sizes less than 10 nm. The mean diameter of the major peak located between 10–100 nm increased dramatically (Fig. 4B) within an hour of Na_3Ctr addition and then stabilized at ≈57 nm after 3 hours. The latter phenomenon agrees with the TEM result in Fig. 3F, which shows that at this point the reaction progress has neared completion of the "cleave" process. Interestingly, there is no evidence in either Fig. 4A or B of spherical networks with size in excess of 100 nm, which suggests that the large networks may have formed during TEM sample preparation. Capillary drying forces are well known to result in enhanced nanoparticle association following drop drying.[80] The association between solution

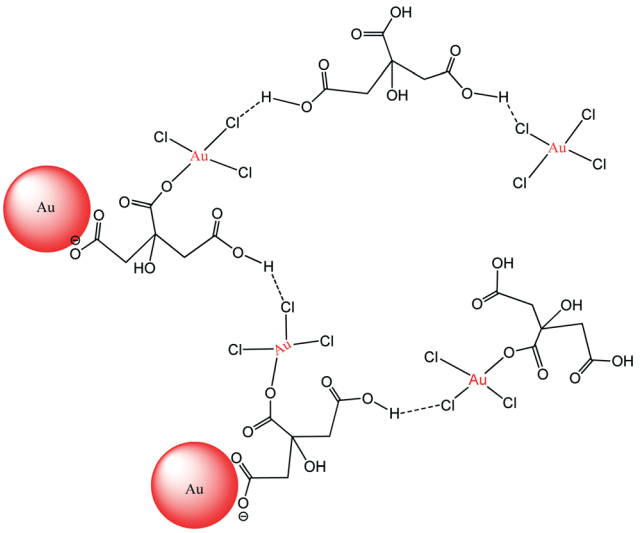

Scheme 1 Reactions among Au seeds, citrate and $AuCl_4^-$ after initial mixing.

phase Au^{III} and the AuNPs is reflected in the absorption spectra in Fig. 4C. There was a board absorption at wavelengths >600 nm that increased in magnitude as time increased from t = 2 min to t = 92 min. This phase of the particle size evolution corresponds to Fig. 3A–D, during which the AuNPs form fluffy networks. The broadening of the LSPR peak in the region >600 nm (Fig. 4C) and the increased absorbance at 700 nm (Fig. 4C inset) corresponds to these fluffy networks. After 92 minutes, a sharp red-shift in the LSPR peak was observed (Fig. 4C), which has been referred to as "turnover" in the literature.[81] The "turnover" point at t = 92 min supports the structure/size change from Fig. 3D to E, during which the fluffy networked structure gave way to discrete AuNPs, which also corresponds to the decreased absorbance at 700 nm (Fig. 4C inset).

Reaction supernatants separated by centrifugation at each reaction time were analyzed by UV-vis spectroscopy and ICP-MS. As shown in Fig. 5, the absorbance at ≈218 nm, which corresponds to unreacted Au^{III},[82] decreases rapidly after the initial mixing of the reagents, stabilizes for approximately 30 minutes, and then decreases linearly with time. Compared to the initial Au^{III} peak intensity at 218 nm, ≈30% of added Au^{III} was reduced after the initial mixing of the reagents. In contrast, over this initial period, ≈93% of total Au was detected by ICP-MS in the reaction supernatant, thus suggesting the presence of an intermediate reduced product of Au^{III} (*i.e.*, Au^{I}) or very small AuNPs. Such a result is consistent with rapid coordination between the carboxylates and Au^{III} and association of these complexes with the Au seeds (*i.e.*, the clusters of seeds and Au^{III} shown in Fig. 3A). The Au^{III} concentration was then stable for next 30 minutes. Such a result suggests that the initial oxidation–reduction reaction only takes place in the clusters shown in Fig. 3A and Scheme 1, which is consistent with the change from Fig. 3A to B. After the initial 30 minutes of reaction, both the concentration of Au^{III} and total Au in the supernatant began

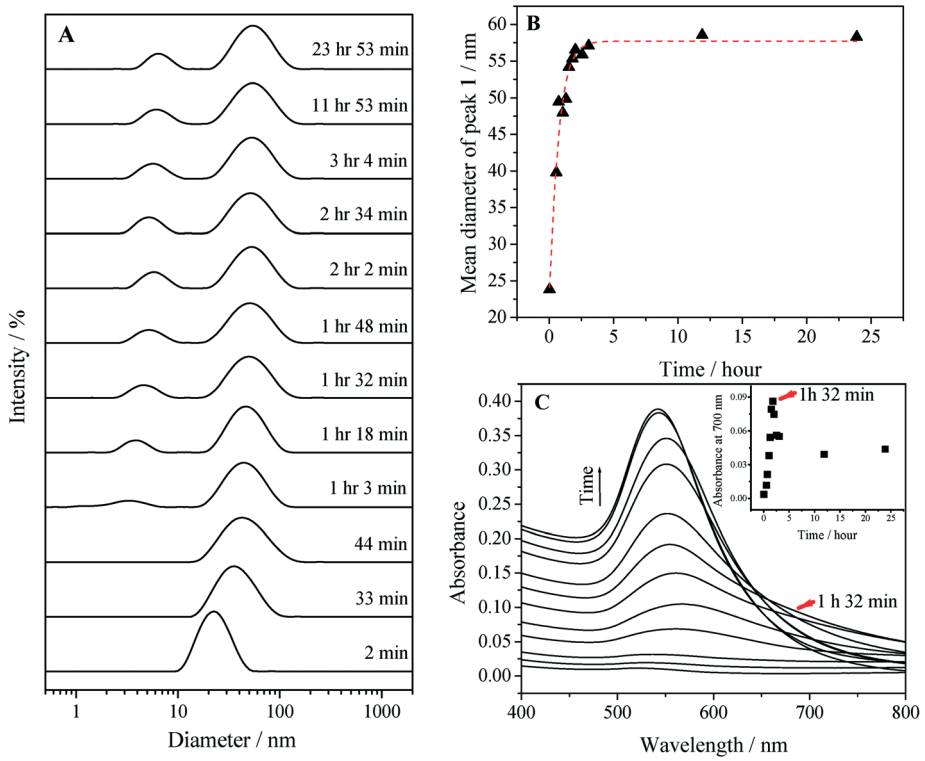

Fig. 4 (A) Size distribution by intensity, (B) mean diameter of peak 1 (located in the range of 10–100 nm in A) and (C) UV-vis absorption spectra obtained at different time stages of seed growth synthesis of AuNPs.

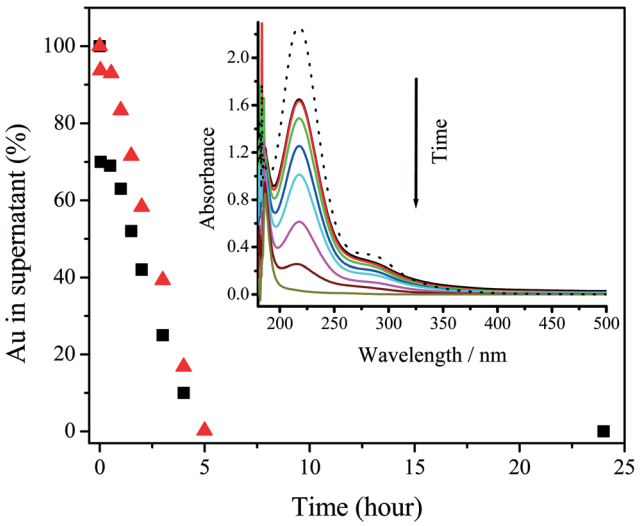

Fig. 5 Time-dependent Au^{III} and Au levels in supernatant as determined by UV-vis (squares) and ICP-MS (triangles). Inset: Corresponding UV absorption spectra. Dash black line is the spectrum of the initial Au^{III} solution. Prior to the UV-vis measurement, all AuNP suspensions were diluted 2× with deionized water.

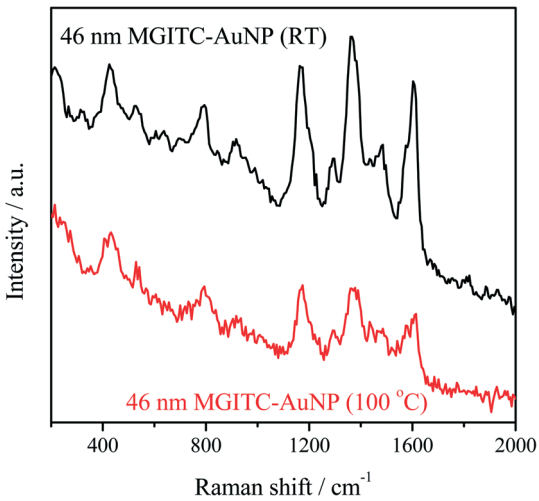

Fig. 6 SERS spectra of MGITC (20 nM) adsorbed on room temperature and 100 °C seed mediated AuNPs under 633 nm excitation. MGITC–AuNPs were prepared by quickly adding ≈1.5 μL of 14 μM MGITC solution to 1 mL AuNP suspension (5.4×10^{10} particle per mL).

to decrease linearly and a total reaction time of ≈5 hours was observed. We used UV-vis spectroscopy to verify that the AuNP growth reaction proceeded according to eqn (11). A mixture of HCl and NaCl with relative concentrations based upon the stoichiometry of eqn (11) was prepared to compare with the UV absorbance of the supernatant of the reaction solution after 5 hours reaction. The near perfect match of the spectra shown in Fig. S8† provides evidence that the stoichiometry of the room temperature seed mediated growth process is reasonably described by eqn (11). Moreover, no residual gold chloride ion was detected in the UV-vis spectrum of the supernatant. As has been previously reported,[31] residual gold exhibits a peak at 218–314 nm in the UV-vis spectra. The absence of this peak in the final UV-vis spectra suggests that there was no residual gold ion. For this reason a 100% reaction yield was assumed, and verified by the ICP-MS results in Fig. 5 To the best of our knowledge this is the first time a reaction stoichiometry has been developed for room-temperature seed-mediated AuNP synthesis.

Evaluation of room temperature seeded AuNPs

The as-prepared AuNPs exhibit exceptional colloidal stability and can be stored at room temperature over several months in spite of their slow agglomeration. The nanoparticles could be easily re-suspended by shaking or sonication. This result suggests these particles can be favorably employed for SERS applications. Fig. 6 compares the surface Raman enhancement of MGITC adsorbed on seed mediated 46 nm AuNPs produced at room temperature with those produced at 100 °C (Fig. S9, ESI†). Importantly, the AuNPs prepared at room temperature exhibit a 2× greater Raman enhancement than AuNPs prepared at 100 °C. We attribute this enhancement to the greater surface roughness of the room temperature AuNPs.[83]

Particles with edges, corners, and branches (*e.g.*, nanorods, nanostars) are quasi-stable at low temperature, but transform into more thermodynamically stable shapes (*i.e.*, spheres) if sufficient thermal energy is provided for atomic reorganization. As shown by TEM imaging (Fig. S9†), the particles prepared at room temperature exhibit more edges and corners than comparable particles prepared at 100 °C thus suggesting the lower synthesis temperature enhances their formation. Because the concentration and volume of AuNPs was constant, the surface area of the particles produced at room temperature will be larger than those synthesized at 100 °C, thus leading to an enhanced surface roughness and higher SERS enhancement relative to AuNPs prepared at 100 °C.

Comparative LCA

The cumulative energy demands (CED) of the AuNP synthesis methods determined by the LCA models are presented in Table 2. The results show that despite the longer reaction time, AuNP synthesis at room temperature has lower CED than synthesis under boiling conditions. The trend of the other impacts across different impact categories matches that of the CED (Fig. S10, ESI†). This result is expected as CED has been shown to correlate well to other environmental impact methods (*e.g.*, EcoIndicator, EcoScarcity, *etc.*).[84] This observation is understandable because the use of fossil fuels (included in CED) is a dominant driver of many environmental impacts.[85]

Uncertainty analysis shows that the differences in the environmental impacts for AuNP synthesis at room temperature and under boiling conditions are statistically significant

Table 2 Cumulative energy demand (CED) for AuNP synthesis at room temperature *vs.* boiling conditions. The CEDs for AuNP syntheses at room temperature and under boiling conditions are 1.25 MJ and 1.54 MJ respectively

Synthesis at room temperature		
Material and energy inputs	Cumulative energy demand (MJ)	% contribution
Chloroauric acid	4.07×10^{-1}	32.59%
Deionized water	8.31×10^{-3}	0.67%
Aqua regia	5.67×10^{-2}	4.54%
AuNP 'seeds'	1.60×10^{-2}	1.28%
Sodium hydroxide	5.27×10^{-7}	4.22×10^{-5}%
Trisodium citrate	5.12×10^{-6}	4.10×10^{-4}%
Stirring	7.61×10^{-1}	60.93%
Total	1.25×10^{-0}	100.00%

Synthesis under boiling conditions		
Material and energy inputs	Cumulative energy demand (MJ)	% contribution
Chloroauric acid	4.07×10^{-1}	26.48%
DI water	8.31×10^{-3}	0.54%
Tap water	1.67×10^{-4}	0.01%
Aqua regia	5.67×10^{-2}	3.69%
AuNP 'seeds'	1.60×10^{-2}	1.04%
Sodium hydroxide	5.27×10^{-7}	3.43×10^{-5}%
Trisodium citrate	5.12×10^{-6}	33.33×10^{-4}%
Heating	9.73×10^{-1}	63.29%
Stirring	7.61×10^{-2}	4.95%
Total	1.54×10^{-0}	100.00%

(Fig. S11†). Although laboratory-scale room temperature synthesis does seem to reduce the energy footprint of AuNP synthesis (compared to the conventional approach at higher temperatures), further studies on scale-up scenarios are recommended, since the environmental footprints are likely to be influenced by yield, energy efficiencies and the available energy sources and fuel-mixes.[86,87] Conventional scale-up of boilers and generators has been shown to follow a power law relationship.[88,89] However, similar relationships for scaling up have not been established for nanoparticle synthesis. Longer reaction times in pilot-scale and commercial-scale setups will involve additional energy demands (*e.g.*, lighting, heat ventilation, air-conditioning *etc.*) that should also be considered in scale up scenarios. The role of regional variability in the energy and water footprints should also be factored into future decisions about nanomaterials industry siting and resource allocation.

Conclusions

A simple room temperature seed mediated preparation route for AuNPs has been demonstrated. Tunability of the AuNP diameter was achieved by simply varying the number concentration of seeds under mild environmental conditions. Such a result shows a promising colorimetric assay using the size-dependent optical property. The continuous surface plasmon oscillations associated with this broad spectral feature gives them broad selection in the future SERS applications. Our reported AuNP synthesis approach helps decrease the rate of AuNP growth due to the milder (room temperature) conditions, thus providing increased opportunities to study a very complicated reaction mechanism. Moreover, this method shows significant reductions in the cradle-to-gate life cycle impacts compared to the previously reported methods that employed boiling conditions.

Acknowledgements

This work was supported by grants from the Virginia Tech Graduate School (Sustainable Nanotechnology Interdisciplinary Graduate Education Program), the Virginia Tech Institute of Critical Technology and Applied Science (ICTAS), and NSF Award CBET-1133746.

References

1 D. Kushnir and B. A. Sandén, Multi-Level Energy Analysis of Emerging Technologies: A Case Study in New Materials for Lithium Ion Batteries, *J. Cleaner Prod.*, 2011, **19**(13), 1405–1416.
2 D. Kushnir and B. A. Sandén, Energy Requirements of Carbon Nanoparticle Production, *J. Ind. Ecol.*, 2008, **12**(3), 360–375.
3 C. J. Murphy, Sustainability as an emerging design criterion in nanoparticle synthesis and applications, *J. Mater. Chem.*, 2008, **18**(19), 2173–2176.
4 M. Grzelczak, J. Pérez-Juste, P. Mulvaney and L. M. Liz-Marzán, Shape control in gold nanoparticle synthesis, *Chem. Soc. Rev.*, 2008, **37**(9), 1783–1791.
5 J. A. Dahl, B. L. S. Maddux and J. E. Hutchison, Toward Greener Nanosynthesis, *Chem. Rev.*, 2007, **107**(6), 2228–2269.
6 J. E. Hutchison, Greener Nanoscience: A Proactive Approach to Advancing Applications and Reducing Implications of Nanotechnology, *ACS Nano*, 2008, **2**(3), 395–402.
7 L. C. McKenzie and J. E. Hutchison, Green nanoscience, *Chim. Oggi*, 2004, **22**(9), 30–33.
8 G. Frens, Controlled nucleation for the regulation of the particle size in monodisperse gold suspensions, *Nature*, 1973, **241**(105), 20–22.
9 J. Turkevich, P. C. Stevenson and J. Hillier, The nucleation and growth processes in the synthesis of colloidal gold, *Discuss. Faraday Soc.*, 1951, **11**, 55–75.
10 M. J. Kogan, N. G. Bastus, R. Amigo, D. Grillo-Bosch, E. Araya, A. Turiel, A. Labarta, E. Giralt and V. F. Puntes, Nanoparticle-Mediated Local and Remote Manipulation of Protein Aggregation, *Nano Lett.*, 2006, **6**(1), 110–115.
11 M.-C. Daniel and D. Astruc, Gold Nanoparticles: Assembly, Supramolecular Chemistry, Quantum-Size-Related Properties, and Applications toward Biology, Catalysis and Nanotechnology, *Chem. Rev.*, 2004, **104**(1), 293–346.
12 N. G. Bastus, E. Sanchez-Tillo, S. Pujals, C. Farrera, C. Lopez, E. Giralt, A. Celada, J. Lloberas and V. Puntes, Homogeneous Conjugation of Peptides onto Gold Nanoparticles Enhances Macrophage Response, *ACS Nano*, 2009, **3**(6), 1335–1344.

13 E. E. Connor, J. Mwamuka, A. Gole, C. J. Murphy and M. D. Wyatt, Gold nanoparticles are taken up by human cells but do not cause acute cytotoxicity, *Small*, 2005, **1**(3), 325–327.
14 Y.-S. Chen, Y.-C. Hung, I. Liau and G. S. Huang, Assessment of the in vivo toxicity of gold nanoparticles, *Nanoscale Res. Lett.*, 2009, **4**(8), 858–864.
15 T. S. Hauck, A. A. Ghazani and W. C. W. Chan, Assessing the effect of surface chemistry on gold nanorod uptake, toxicity and gene expression in mammalian cells, *Small*, 2008, **4**(1), 153–159.
16 S. D. Brown, P. Nativo, J.-A. Smith, D. Stirling, P. R. Edwards, B. Venugopal, D. J. Flint, J. A. Plumb, D. Graham and N. J. Wheate, Gold Nanoparticles for the Improved Anticancer Drug Delivery of the Active Component of Oxaliplatin, *J. Am. Chem. Soc.*, 2010, **132**(13), 4678–4684.
17 S. Bhattacharyya, R. Bhattacharya, S. Curley, M. A. McNiven and P. Mukherjee, Nanoconjugation modulates the trafficking and mechanism of antibody induced receptor endocytosis, *Proc. Natl. Acad. Sci. U. S. A.*, 2010, **107**(33), 14541–14546.
18 A. G. Tkachenko, H. Xie, D. Coleman, W. Glomm, J. Ryan, M. F. Anderson, S. Franzen and D. L. Feldheim, Multifunctional gold nanoparticle-peptide complexes for nuclear targeting, *J. Am. Chem. Soc.*, 2003, **125**(16), 4700–4701.
19 B. Kang, M. A. Mackey and M. A. El-Sayed, Nuclear Targeting of Gold Nanoparticles in Cancer Cells Induces DNA Damage, Causing Cytokinesis Arrest and Apoptosis, *J. Am. Chem. Soc.*, 2010, **132**(5), 1517–1519.
20 E.-K. Oh, J. B. Delehanty, K. E. Sapsford, K. Susumu, R. Goswami, J. B. Blanco-Canosa, P. E. Dawson, J. Granek, M. Shoff, Q. Zhang, P. L. Goering, A. Huston and I. L. Medintz, Cellular Uptake and Fate of PEGylated Gold Nanoparticles Is Dependent on Both Cell-Penetration Peptides and Particle Size, *ACS Nano*, 2011, **5**(8), 6434–6448.
21 G. F. Paciotti, D. G. I. Kingston and L. Tamarkin, Colloidal gold nanoparticles: a novel nanoparticle platform for developing multifunctional tumor-targeted drug delivery vectors, *Drug Dev. Res.*, 2006, **67**(1), 47–54.
22 V. K. K. Upadhyayula, Functionalized gold nanoparticle supported sensory mechanisms applied in detection of chemical and biological threat agents: A review, *Anal. Chim. Acta*, 2012, **715**, 1–18.
23 J. Wang, Nanomaterial-based amplified transduction of biomolecular interactions, *Small*, 2005, **1**(11), 1036–1043.
24 P. He, L. Shen, R. Liu, Z. Luo and Z. Li, Direct Detection of N2-Agonists by Use of Gold Nanoparticle-Based Colorimetric Assays, *Anal. Chem.*, 2012, **83**(18), 6988–6995.
25 T. Pellegrino, S. Kudera, T. Liedl, A. M. Javier, L. Manna and W. J. Parak, On the development of colloidal nanoparticles towards multifunctional structures and their possible use for biological applications, *Small*, 2005, **1**(1), 48–63.
26 M. Scampicchio, J. Wang, A. J. Blasco, A. S. Arribas, S. Mannino and A. Escarpa, Nanoparticle-Based Assays of Antioxidant Activity, *Anal. Chem.*, 2006, **78**(6), 2060–2063.
27 I. Willner, R. Baron and B. Willner, Growing metal nanoparticles by enzymes, *Adv. Mater.*, 2006, **18**(9), 1109–1120.
28 C. Burda, X. Chen, R. Narayanan and M. A. El-Sayed, Chemistry and Properties of Nanocrystals of Different Shapes, *Chem. Rev.*, 2005, **105**(4), 1025–1102.
29 B. Nikoobakht and M. A. El-Sayed, Preparation and growth mechanism of gold nanorods (NRs) using seed-mediated growth method, *Chem. Mater.*, 2003, **15**(10), 1957–1962.
30 C. J. Murphy and N. R. Jana, Controlling the aspect ratio of inorganic nanorods and nanowires, *Adv. Mater.*, 2002, **14**(1), 80–82.
31 X. Ji, X. Song, J. Li, Y. Bai, W. Yang and X. Peng, Size Control of Gold Nanocrystals in Citrate Reduction: The Third Role of Citrate, *J. Am. Chem. Soc.*, 2007, **129**(45), 13939–13948.
32 N. R. Jana, L. Gearheart and C. J. Murphy, Seeding growth for size control of 5–40 nm diameter gold nanoparticles, *Langmuir*, 2001, **17**(22), 6782–6786.
33 J. Kimling, M. Maier, B. Okenve, V. Kotaidis, H. Ballot and A. Plech, Turkevich Method for Gold Nanoparticle Synthesis Revisited, *J. Phys. Chem. B*, 2006, **110**(32), 15700–15707.
34 G. Frens, Controlled nucleation for the regulation of the particle size in monodisperse gold suspensions, *Nature (London), Phys. Sci.*, 1973, **241**(105), 20–22.
35 M. K. Chow and C. F. Zukoski, Gold sol formation mechanisms: role of colloidal stability, *J. Colloid Interface Sci.*, 1994, **165**(1), 97–109.
36 J. Turkevich, P. C. Stevenson and J. Hillier, The formation of colloidal gold, *J. Phys. Chem.*, 1953, **57**, 670–673.
37 I. Ojea-Jimenez, F. M. Romero, N. G. Bastus and V. Puntes, Small Gold Nanoparticles Synthesized with Sodium Citrate and Heavy Water: Insights into the Reaction Mechanism, *J. Phys. Chem. C*, 2010, **114**(4), 1800–1804.
38 A. Henglein and M. Giersig, Formation of colloidal silver nanoparticles. Capping action of citrate, *J. Phys. Chem. B*, 1999, **103**(44), 9533–9539.
39 S. Kumar, K. S. Gandhi and R. Kumar, Modeling of formation of gold nanoparticles by citrate method, *Ind. Eng. Chem. Res.*, 2007, **46**(10), 3128–3136.
40 T. K. Sau and C. J. Murphy, Room Temperature, High-Yield Synthesis of Multiple Shapes of Gold Nanoparticles in Aqueous Solution, *J. Am. Chem. Soc.*, 2004, **126**(28), 8648–8649.
41 M. N. Nadagouda and R. S. Varma, Green synthesis of silver and palladium nanoparticles at room temperature using coffee and tea extract, *Green Chem.*, 2008, **10**(8), 859–862.
42 S. D. Perrault and W. C. W. Chan, Synthesis and Surface Modification of Highly Monodispersed, Spherical Gold Nanoparticles of 50–200 nm, *J. Am. Chem. Soc.*, 2009, **131**(47), 17042–17043.
43 C. Ziegler and A. Eychmüller, Seeded Growth Synthesis of Uniform Gold Nanoparticles with Diameters of 15–300 nm, *J. Phys. Chem. C*, 2011, **115**(11), 4502–4506.
44 P. T. Anastas and J. C. Warner, *Green chemistry: theory and practice*, Oxford University Press, USA, 2000.
45 P. Pati, S. McGinnis and P. J. Vikesland, Life Cycle Assessment of "Green" Nanoparticle Synthesis Methods, *Environ. Eng. Sci.*, 2014, **31**(7), 410–420.

46 T. Walser, E. Demou, D. J. Lang and S. Hellweg, Prospective Environmental Life Cycle Assessment of Nanosilver T-Shirts, *Environ. Sci. Technol.*, 2011, **45**(10), 4570–4578.
47 C. Bauer, J. Buchgeister, R. Hischier, W. R. Poganietz, L. Schebek and J. Warsen, Towards a Framework for Life Cycle Thinking in the Assessment of Nanotechnology, *J. Cleaner Prod.*, 2008, **16**(8–9), 910–926.
48 H. C. Kim and V. Fthenakis, Life Cycle Energy and Climate Change Implications of Nanotechnologies, *J. Ind. Ecol.*, 2013, **17**(4), 528–541.
49 Q. Li, S. McGinnis, C. Sydnor, A. Wong and S. Renneckar, Nanocellulose Life Cycle Assessment, *ACS Sustainable Chem. Eng.*, 2013, **1**(8), 919–928.
50 V. K. K. Upadhyayula, D. E. Meyer, M. A. Curran and M. A. Gonzalez, Evaluating the Environmental Impacts of a Nano-Enhanced Field Emission Display Using Life Cycle Assessment: A Screening-Level Study, *Environ. Sci. Technol.*, 2013, **48**(2), 1194–1205.
51 H. Chen, X. Kou, Z. Yang, W. Ni and J. Wang, Shape- and Size-Dependent Refractive Index Sensitivity of Gold Nanoparticles, *Langmuir*, 2008, **24**(10), 5233–5237.
52 X. Liu, M. Atwater, J. Wang and Q. Huo, Extinction coefficient of gold nanoparticles with different sizes and different capping ligands, *Colloids Surf., B*, 2007, **58**(1), 3–7.
53 W. Haiss, N. T. K. Thanh, J. Aveyard and D. G. Fernig, Determination of size and concentration of gold nanoparticles from UV-vis spectra, *Anal. Chem.*, 2007, **79**(11), 4215–4221.
54 N. G. Bastus, J. Comenge and V. Puntes, Kinetically Controlled Seeded Growth Synthesis of Citrate-Stabilized Gold Nanoparticles of up to 200 nm: Size Focusing *versus* Ostwald Ripening, *Langmuir*, 2011, **27**(17), 11098–11105.
55 J. B. Guinée, R. Heijungs, G. Huppes, A. Zamagni, P. Masoni, R. Buonamici, T. Ekvall and T. Rydberg, Life Cycle Assessment: Past, Present and Future, *Environ. Sci. Technol.*, 2011, **45**(1), 90–96.
56 R. Frischknecht, N. Jungbluth, H.-J. Althaus, G. Doka, R. Dones, T. Heck, S. Hellweg, R. Hischier, T. Nemecek and G. Rebitzer, The ecoinvent database: Overview and methodological framework (7 pp), *Int. J. Life Cycle Assess.*, 2005, **10**(1), 3–9.
57 P. Pati, S. McGinnis and P. J. Vikesland, Life Cycle Assessment of "Green" Nanoparticle Synthesis Methods, *Environ. Eng. Sci.*, 2014, **31**(7), 410–420.
58 R. Frischknecht, N. Jungbluth, H. J. Althaus, C. Bauer, G. Doka, R. Dones, R. Hischier, S. Hellweg, S. Humbert and T. Köllner, Implementation of life cycle impact assessment methods, *3; EcoInvent Report: 2007*, 2007.
59 M. L. Machesky, W. O. Andrade and A. W. Rose, Adsorption of gold(III)-chloride and gold(I)-thiosulfate anions by goethite, *Geochim. Cosmochim. Acta*, 1991, **55**(3), 769–776.
60 D. V. Goia and E. Matijevic, Tailoring the particle size of monodispersed colloidal gold, *Colloids Surf., A*, 1999, **146**(1–3), 139–152.
61 S. Wang, K. Qian, X. Bi and W. Huang, Influence of Speciation of Aqueous HAuCl4 on the Synthesis, Structure, and Property of Au Colloids, *J. Phys. Chem. C*, 2009, **113**(16), 6505–6510.
62 K. R. Brown, D. G. Walter and M. J. Natan, Seeding of colloidal Au nanoparticle solutions. 2. Improved control of particle size and shape, *Chem. Mater.*, 2000, **12**(2), 306–313.
63 K. R. Brown, D. G. Walter and M. J. Natan, Seeding of colloidal Au nanoparticle solutions. 2. Improved control of particle size and shape, *Chem. Mater.*, 2000, **12**(2), 306–313.
64 J. C. Thomas, The determination of log normal particle size distributions by dynamic light scattering, *J. Colloid Interface Sci.*, 1987, **117**(1), 187–192.
65 B. N. Khlebtsov and N. G. Khlebtsov, On the measurement of gold nanoparticle sizes by the dynamic light scattering method, *Colloid J.*, 2011, **73**(1), 118–127.
66 M. S. Hull, P. Chaurand, J. Rose, M. Auffan, J.-Y. Bottero, J. C. Jones, I. R. Schultz and P. J. Vikesland, Filter-Feeding Bivalves Store and Biodeposit Colloidally Stable Gold Nanoparticles, *Environ. Sci. Technol.*, 2011, **45**(15), 6592–6599.
67 W. Leng and P. J. Vikesland, MGITC Facilitated Formation of AuNP Multimers, *Langmuir*, 2014, **30**(28), 8342–8349.
68 L. M. Liz-Marzan, Tailoring Surface Plasmons through the Morphology and Assembly of Metal Nanoparticles, *Langmuir*, 2006, **22**(1), 32–41.
69 C. J. Murphy, T. K. San, A. M. Gole, C. J. Orendorff, J. X. Gao, L. Gou, S. E. Hunyadi and T. Li, Anisotropic metal nanoparticles: Synthesis, assembly, and optical applications, *J. Phys. Chem. B*, 2005, **109**(29), 13857–13870.
70 K. L. Kelly, E. Coronado, L. L. Zhao and G. C. Schatz, The Optical Properties of Metal Nanoparticles: The Influence of Size, Shape, and Dielectric Environment, *J. Phys. Chem. B*, 2003, **107**(3), 668–677.
71 J. P. Wilcoxon, J. E. Martin and P. Provencio, Optical properties of gold and silver nanoclusters investigated by liquid chromatography, *J. Chem. Phys.*, 2001, **115**(2), 998–1008.
72 A. C. Kuyper, Oxidation of citric acid, *J. Am. Chem. Soc.*, 1933, **55**, 1722–1727.
73 C. H. Munro, W. E. Smith, M. Garner, J. Clarkson and P. C. White, Characterization of the Surface of a Citrate-Reduced Colloid Optimized for Use as a Substrate for Surface-Enhanced Resonance Raman Scattering, *Langmuir*, 1995, **11**(10), 3712–3720.
74 B. Tang, J. Tao, S. Xu, J. Wang, C. Hurren, W. Xu, L. Sun and X. Wang, Using hydroxy carboxylate to synthesize gold nanoparticles in heating and photochemical reactions and their application in textile coloration, *Chem. Eng. J.*, 2011, **172**(1), 601–607.
75 M. Iosin, P. Baldeck and S. Astilean, Study of tryptophan assisted synthesis of gold nanoparticles by combining UV-vis, fluorescence, and SERS spectroscopy, *J. Nanopart. Res.*, 2010, **12**(8), 2843–2849.
76 J. Turkevich, Colloidal gold. Part I. Historical and preparative aspects, morphology and structure, *Gold Bull.*, 1985, **18**(3), 86–91.

77 J. Turkevich, Colloidal gold. Part II. Color, coagulation, adhesion, alloying and catalytic properties, *Gold Bull.*, 1985, **18**(4), 125–131.

78 J. M. Hull, M. R. Provorse and C. M. Aikens, Formyloxyl Radical-Gold Nanoparticle Binding: A Theoretical Study, *J. Phys. Chem. A*, 2012, **116**(22), 5445–5452.

79 L. Pei, K. Mori and M. Adachi, Formation Process of Two-Dimensional Networked Gold Nanowires by Citrate Reduction of $AuCl_4^-$ and the Shape Stabilization, *Langmuir*, 2004, **20**(18), 7837–7843.

80 X. Chang and P. J. Vikesland, Uncontrolled Variability in the Extinction Spectra of C60 Nanoparticle Suspensions, *Langmuir*, 2013, **29**(31), 9685–9693.

81 S. Peng, J. M. McMahon, G. C. Schatz, S. K. Gray and Y. Sun, Reversing the size-dependence of surface plasmon resonances, *Proc. Natl. Acad. Sci. U. S. A.*, 2010, **107**(33), 14530–14534.

82 J. A. Peck, C. D. Tait, B. I. Swanson and G. E. Brown Jr, Speciation of aqueous gold(III) chlorides from ultraviolet/visible absorption and Raman/resonance Raman spectroscopies, *Geochim. Cosmochim. Acta*, 1991, **55**(3), 671–676.

83 C. E. Talley, J. B. Jackson, C. Oubre, N. K. Grady, C. W. Hollars, S. M. Lane, T. R. Huser, P. Nordlander and N. J. Halas, Surface-Enhanced Raman Scattering from Individual Au Nanoparticles and Nanoparticle Dimer Substrates, *Nano Lett.*, 2005, **5**(8), 1569–1574.

84 M. A. J. Huijbregts, S. Hellweg, R. Frischknecht, H. W. M. Hendriks, K. Hungerbühler and A. J. Hendriks, Cumulative Energy Demand As Predictor for the Environmental Burden of Commodity Production, *Environ. Sci. Technol.*, 2010, **44**(6), 2189–2196.

85 M. A. J. Huijbregts, L. J. A. Rombouts, S. Hellweg, R. Frischknecht, A. J. Hendriks, D. van de Meent, A. M. J. Ragas, L. Reijnders and J. Struijs, Is Cumulative Fossil Energy Demand a Useful Indicator for the Environmental Performance of Products?, *Environ. Sci. Technol.*, 2006, **40**(3), 641–648.

86 M. Shibasaki, M. Fischer and L. Barthel, Effects on Life Cycle Assessment—Scale Up of Processes, in *Advances in Life Cycle Engineering for Sustainable Manufacturing Businesses*, ed. S. Takata and Y. Umeda, Springer, London, 2007, pp. 377–381.

87 M. Shibasaki, N. Warburg and P. Eyerer, in *Upscaling effect and Life Cycle Assessment*, 2006.

88 M. Caduff, M. A. J. Huijbregts, H.-J. Althaus and A. J. Hendriks, Power-Law Relationships for Estimating Mass, Fuel Consumption and Costs of Energy Conversion Equipments, *Environ. Sci. Technol.*, 2011, **45**(2), 751–754.

89 M. Caduff, M. A. J. Huijbregts, A. Koehler, H.-J. Althaus and S. Hellweg, Scaling Relationships in Life Cycle Assessment, *J. Ind. Ecol.*, 2014, **18**(3), 393–406.